



UNIVERSITY OF LEEDS

This is a repository copy of *Thermal stability of C-S-H phases and applicability of Richardson and Groves' and Richardson C-(A)-S-H(I) models to synthetic C-S-H.*

White Rose Research Online URL for this paper:

<https://eprints.whiterose.ac.uk/109873/>

Version: Accepted Version

---

**Article:**

Rodriguez, ET, Garbev, K, Merz, D et al. (2 more authors) (2017) Thermal stability of C-S-H phases and applicability of Richardson and Groves' and Richardson C-(A)-S-H(I) models to synthetic C-S-H. *Cement and Concrete Research*, 93. pp. 45-56. ISSN 0008-8846

<https://doi.org/10.1016/j.cemconres.2016.12.005>

---

© 2016 Published by Elsevier Ltd. Licensed under the Creative Commons Attribution-NonCommercial-NoDerivatives 4.0 International <http://creativecommons.org/licenses/by-nc-nd/4.0/>

**Reuse**

Items deposited in White Rose Research Online are protected by copyright, with all rights reserved unless indicated otherwise. They may be downloaded and/or printed for private study, or other acts as permitted by national copyright laws. The publisher or other rights holders may allow further reproduction and re-use of the full text version. This is indicated by the licence information on the White Rose Research Online record for the item.

**Takedown**

If you consider content in White Rose Research Online to be in breach of UK law, please notify us by emailing [eprints@whiterose.ac.uk](mailto:eprints@whiterose.ac.uk) including the URL of the record and the reason for the withdrawal request.



[eprints@whiterose.ac.uk](mailto:eprints@whiterose.ac.uk)  
<https://eprints.whiterose.ac.uk/>

# Thermal stability of C-S-H phases and applicability of Richardson and Groves' and Richardson C-(A)-S-H(I) models to synthetic C-S-H

Elena Tajuelo Rodriguez <sup>a,1</sup>, Krassimir Garbev <sup>b</sup>, Daniela Merz <sup>b</sup>, Leon Black <sup>a</sup>, Ian G. Richardson <sup>a\*</sup>

<sup>a</sup> School of Civil Engineering, University of Leeds, Leeds, LS2 9JT, UK

<sup>b</sup> Karlsruhe Institute of Technology, Institute for Technical Chemistry (ITC), Hermann-von-Helmholtz-Platz 1, 76344 Eggenstein-Leopoldshafen, Germany

## Abstract

Synthetic C-S-H samples prepared with bulk C/S ratios from 0.75 to 1.5 were analyzed by coupled TG/DSC/FTIR and in-situ XRD while heating, in order to correlate observed weight loss curves with the kinetics of evolved gases, and to investigate the transformations C-S-H→ $\beta$ -wollastonite→ $\alpha$ -wollastonite. The temperature of the transformation to  $\beta$ -wollastonite increased with increasing C/S. The temperature for the transformation from  $\beta$ - to  $\alpha$ -wollastonite meanwhile decreased with increasing C/S; indicating that excess CaO stabilized the  $\alpha$ -polymorph. The transformation C-S-H→ $\beta$ -wollastonite was accompanied by the formation of  $\alpha$ -L C<sub>2</sub>S for C/S > 1. In the case of C-S-H with C/S = 1.5, both  $\beta$ -C<sub>2</sub>S and rankinite were formed and then decomposed before the transformation to  $\beta$ -wollastonite and  $\alpha$ -L C<sub>2</sub>S. C-S-H with low C/S was found to be more stable upon heating. The chemical structural models of Richardson and Groves' and Richardson C-A-S-H(I) were used to obtain the structural-chemical formulae.

Keywords: A. Calorimetry, B. Calcium Silicate Hydrate (C-S-H), B. Spectroscopy, B. Thermal Analysis, B. X-ray diffraction

## 1. Introduction

C-S-H (calcium silicate hydrate) is the principal binding phase of Portland cement and concrete, and hence is responsible for its strength. It forms upon the hydration of

---

<sup>1</sup> Present address: Oak Ridge National Laboratory, One Bethel Valley Road, Oak Ridge, TN 37831, USA, email: tajuelorodre@ornl.gov

\* Corresponding author: Ian. G. Richardson, i.g.richardson@leeds.ac.uk

cement and it is the most voluminous hydration phase. Its C/S ratio ranges from 1.3 to 2.1 [1] with a mean of 1.75 [2] in neat Portland cement. Due to the partial replacement of cement with supplementary cementitious materials and to ageing, its composition varies greatly, exhibiting C/S ratios in the range 0.7-2.1 [3]. C-S-H, despite being described as near amorphous, has some structural similarities with natural minerals such as tobermorite [4] and jennite [5], and with other more ordered semicrystalline synthetic phases such as C-S-H(I) [6] (of low C/S ratio) and C-S-H(II) [6, 7] (of high C/S ratio). The thermal stability of C-S-H is key to understand the degradation of cement pastes at high temperatures. Changes in nanostructure and morphology of C-S-H after being subject to elevated temperatures cause an increase in porosity and degrade the mechanical properties of cement pastes [8].

From thermal analysis and XRD post-heating it is known that C-S-H (I) transforms into wollastonite ( $\text{CaSiO}_3$ ) above  $800^\circ\text{C}$  [9-11]. The temperature for the transformation increases with the C/S ratio [9-12] and thus depends on the C-S-H structure, in particular on the occupancy of the interlayer [13]. To calculate the amount of calcium in the interlayer, as well as derive an average composition and chemical structural formulae of C-S-H, a chemical structural model is needed. One of the first to be proposed was that of Taylor [14], which considers C-S-H with high C/S ratio (from Portland cement or  $\text{C}_3\text{S}$  pastes) as a combination of imperfect layers of jennite and a smaller proportion of imperfect layers of tobermorite. This model can reach minimum and maximum C/S ratios of 0.83 and 2.25. Richardson and Groves' presented a more flexible model [15] that includes two viewpoints combining structural units of different phases: tobermorite/jennite (T/J) and tobermorite/calcium hydroxide (T/CH). This model can reach C/S ratios from 0.67 to 2.5. It was further extended to include minor elements [16], such as aluminum or alkalis, and has been applied to explain the

structure of C-S-H in a wide range of cementitious systems [17]. The schematic figures presented in [17] for the tobermorite-based structural units in these models (e.g. Fig. 27) were produced using the crystal structure of an orthotobermorite. However, Richardson has proved that clinotobermorite is a better choice with his recent C-(A)-S-H(I) model [18], since it is only possible to build a plausible silicate dimer in terms of crystal-chemical reasoning starting from a clinotobermorite structure. This hypothetical dimer presents ribbons of Ca-O octahedra which are very similar to those present in CH. This similarity could explain the intergrowth of CH layers with the dimeric structures and justify the T/CH view point in Richardson and Groves' model. The Richardson C-(A)-S-H(I) model was built in accordance with available data regarding changes in basal spacing with water content and C/S ratio, and other structural changes in the structure of C-S-H with C/S ratio. The model provides expressions to calculate the C/S ratio of C-S-H knowing the fraction of vacant tetrahedral sites, or simply the percentages of the silicate species. Despite being derived using different tobermorite structural units, both Richardson and Groves' and Richardson C-(A)-S-H(I) models represent equivalent formulations based on the same charge-balance arguments.

Most traditional thermal analyses of C-S-H have been done up to 1000°C and behavior at higher temperatures has not received much attention. The main purpose of this study was to investigate the thermal stability of C-S-H(I) phases up to 1400°C and monitor the phase transformations (C-S-H →  $\beta$ -wollastonite →  $\alpha$ -wollastonite) upon heating for bulk C/S ratios from 0.75 to 1.5. A coupled TG/DSC/FTIR (Thermogravimetry/ Differential Scanning Calorimetry/ Fourier Transformed Infrared Spectroscopy) technique was used to study C-S-H. FTIR has been used to study the structure of C-S-H [19], but has never been used to monitor the gases that are released from C-S-H while heating as a complementary technique to thermogravimetry. XRD was employed to check the purity

of the samples and to obtain the basal spacing. The basal spacing as a function of C/S was then compared with data in literature and with the derived basal spacing for the model structures in Richardson C-(A)-S-H(I) model. *In situ* XRD up to 1100°C was used to gain additional information, such as the crystallization and decomposition of other phases, and to study the drop of the intensity of the main C-S-H reflection with temperature. Richardson and Groves' model was used to yield chemical structural formulae for the average composition of C-S-H samples taking into account the water content from FTIR, average C/S measured by TEM [20] and MCL calculated through NMR [20]. The amount of interlayer Ca<sup>2+</sup> per silicate tetrahedral site was obtained through Richardson C-(A)-S-H(I) model to link the occupancy of the interlayer to the temperature transformation to wollastonite. Structural data from the samples was also compared with a constraint that expresses mean silicate chain length (MCL) in terms of C/S ratio in Richardson C-(A)-S-H(I) model.

## **2. Materials and methods**

### **2.1 Synthesis of C-S-H**

The synthesis was performed mechanochemically, as described by Garbev et al. [21], and as used by Saito [22] to synthesize various calcium silicate hydrates. CaO and SiO<sub>2</sub> (Aerosil 200) were mixed in a roller mill w/s=8 (water-to-solid ratio). CaO was obtained by roasting CaCO<sub>3</sub> for 3 hours at 900°C. The amount of silica used for each sample was 5g, and the amount of CaO was such so that the bulk C/S ratios of the mixtures were 0.75, 0.83, 1, 1.25, 1.33 and 1.5. The mixtures were poured into roller mill pots inside a glovebox under a nitrogen atmosphere to prevent carbonation. The pots were sealed in the glovebox to ensure no entrance of air. The mixtures were milled with on-off cycles of 20-10 min respectively for 36 hours. The pauses were necessary to

prevent overheating. After milling, the slurries were rinsed with ethanol and filtered in a Buchner funnel inside a glovebox. They were then dried under a continuous nitrogen gas flow of 20 cm<sup>3</sup>/min over a hot plate at 60°C in a glovebox. All the samples were stored in sealed containers prior to analyses.

## 2.2 TG/DSC/FTIR

A thermo balance Jupiter 449-F3 (Netzsch, Selb, Germany), equipped with a DSC sample carrier, and coupled to a Bruker Tensor 27 FTIR Spectrometer (Bruker optics, Ettlingen, Germany) was used for TG/DSC/FTIR experiments. The transfer line connecting the thermo balance and the FTIR Spectrometer had a length of 100 cm and a PTFE (Polytetrafluoroethylene) inlet. The TG-FTIR unit had an optical path length of 123 mm, and KBr and ZnSe-windows. The transfer line and the FTIR cell were heated to 200°C to prevent sorption of evolved species during analysis. A Pt/Rh crucible was used to place 10-30 mg of each sample. The experiments were done at a heating rate of 10°C /min with nitrogen as a purge gas at a flow of 70 ml/min (including 20 ml of balance protective gas). The FTIR resolution was 4cm<sup>-1</sup> with a scan rate of 32. The spectra were recorded every 15s. The FTIR baseline was measured prior to the introduction of samples in the system to avoid weight loss of the samples while measuring the baseline. Residual atmospheric water and CO<sub>2</sub> were thus detected in the first few minutes of the experiments. Their signal was removed for the quantification of the spectra. Bruker OPUS software and Netzsch Proteus software were used to evaluate the spectra. The quantification method was based on the simultaneous control of the purge gas flow after an external calibration according to Merz *et al.* [23]. A certified test gas of CO<sub>2</sub> in N<sub>2</sub> (certified by Basi, Rastatt, Germany) was measured in the FTIR cell under identical conditions to the experiments for the calibration of CO<sub>2</sub>. Thermal degradation of 20 samples of calcium oxalate monohydrate was used for the calibration

of H<sub>2</sub>O. For the concentration ranges used, all absorption response curves could be described by linear fitting and the Beer-Lambert Law was valid.

Temperature calibration and enthalpy calibration was conducted on standard materials In, Sn, Bi, Zn, Al, Ag and Au. The enthalpies ( $\Delta H$ ) of transformations to CS, C<sub>2</sub>S and C<sub>3</sub>S<sub>2</sub> were calculated by the determination of the area of the exothermic event in the DSC curve (or the partial area where necessary) by the tangential method. The results (in J/g) were calculated in kJ/mol multiplying by the molar mass.

The heat capacity ( $\Delta C_p$ ) for the transformation C-S-H  $\rightarrow$   $\beta$ -wollastonite was measured as the difference in the heat flow (DSC, signal measured in mW/mg) between two temperatures ( $T_2$  after transition,  $T_1$  before transition) in the reaction range at known mass of the sample and at a certain heating rate (in this case 10°C/s). The choice of  $T_2$  and  $T_1$  was constrained by using the inflection points of the first derivative of the DSC curve. Due to the different transition temperatures observed in the different samples, the following ranges were set: for C/S=0.75 and 0.83 -790-870°C, C/S=1.0 – 825-845°C, C/S=1.25 – 845-925°C, C/S=1.33 – 870-940°C, and C/S=1.5 -880-920°C.

### **2.3 XRD**

Samples were crushed using a pestle in a mortar, with the resultant powders back-filled in sample holders to ensure a uniform surface for X-ray exposure. The XRD patterns were taken under continuous spinning in a Panalytical X'Pert Pro diffractometer (Panalytical, Almelo, Netherlands) with a Cu K $\alpha$  source operated at 40 kV and 40 mA. A 10 mm mask and a 10 mm antiscatter slit were used. The minimum and maximum values for  $2\theta$  were 4° and 80° respectively. The step size was 0.033° and the time per step 95s, yielding a total time of  $\approx$  30 min for each scan. The patterns were compared

with reference patterns from the Chemical Database Service to identify traces from other phases.

## **2.4 *In situ* XRD**

In-situ heating experiments were performed on selected samples ( $C/S = 0.75, 1.0, 1.25$  and  $1.5$ ) with  $Cu K_{\alpha}$  radiation on a Bruker-AXS D8 Advance diffractometer (Bruker-AXS, Karlsruhe, Germany). High-temperature experiments (every  $10^{\circ}C$  over the range  $30-300^{\circ}C$  and every  $50^{\circ}C$  over the range  $350-1100^{\circ}C$ ) were performed with a high-temperature camera HTK 1200 (Anton Paar Germany GmbH, Mainz, Germany) and Position Sensitive Detector (Braun, Garching, Germany). The temperature was calibrated with boron nitride (Mathey Reagent) after the method of Pease [24]. The measurements were performed with a step width of  $0.0135^{\circ} 2\theta$  and  $0.6$  sec/step at a heating rate of  $1^{\circ}C/1$  min after equilibration for 20 min at the desired temperature.

## **3. Results and discussion**

### **3.1 XRD**

The XRD patterns obtained from the C-S-H samples are shown in Fig. 1, together with a reference pattern for portlandite [25] from the Chemical Database service. Note that the bulk  $C/S$  ratios from the preparations are indicated in the plot, but the measured compositions for the samples are published elsewhere [20]. All traces show reflections typical for C-S-H(I) [26]. The samples were single phase up to  $C/S = 1.33$ . A trace of portlandite was found in the sample with bulk  $C/S = 1.5$  (reflections at  $2\theta \approx 18^{\circ}, 33^{\circ}, 47^{\circ}$  and  $50.7^{\circ}$ ). The basal reflection (first low angle reflection) was visible in all the samples. This reflection is a sign of 3D ordering; and it shifted towards higher angles with increasing  $C/S$ , indicating a lower basal or interlayer spacing. This agrees with other reported data that show a decrease in basal spacing of C-S-H with  $C/S$  [27-29].

There are differing views about the reasons behind the decrease in basal spacing with increasing C/S; one of them supports the removal of silicate bridging tetrahedra and the inclusion of  $\text{Ca}^{2+}$  ions in the interlayer as mechanisms [21], while the other supports an interstratification of layers of tobermorite dimers and tobermorite infinite layers ( $T_2$  and  $T_{\text{inf}}$  in [18]) with increasing number of dimeric layers as the C/S increases [18]. The basal reflection also increased in intensity with increasing C/S ratio, which is a further indication of improved structural ordering with increasing Ca content. This has not always been observed in the past, and the opposite case has also been reported [30]. The appearance of a shoulder at  $2\theta \approx 30^\circ$  for high C/S ratio, observed in Fig. 1, was pointed out as another sign of increasing structural order by Garbev *et al.* [21]. Their conclusion opposed Cong and Kirkpatrick [29] who supported a decrease in structural ordering with increasing C/S due to the decrease in the number of resolvable peaks. The flattening of the reflection at  $2\theta \approx 16^\circ$  was observed in Fig. 1. Grangeon *et al.* [31], have recently shown that the decrease in intensity of the reflection at  $2\theta \approx 16^\circ$  relative to the intensity of the reflection at  $2\theta \approx 29^\circ$ , rather than signifying a decrease in structural ordering with C/S, is an effect of the decreased occupancy of the Si bridging sites with increasing C/S. The decrease in intensity of this reflection is also consistent with the structures given by Richardson C-(A)-S-H(I) model, i.e. the peak in this position diminishes in intensity on the calculated XRD patterns as the MCL gets shorter (see Fig. 16 in [18]). Another feature that would favor increased structural ordering, which has remained unnoticed in the past, is the flattening of the hump at  $2\theta \approx 44^\circ$ . Such humps may be associated with amorphous materials; therefore the observed increase in intensity of the basal reflection, accompanied by a decrease in intensity of the aforementioned hump, would support Garbev's *et al.* [21] conclusions. Furthermore, the main reflection at  $\approx 29^\circ$  is sharpened with increasing C/S ratio, which is also evidence

for improved structural ordering. A sharpening of this reflection (decrease in FWHM) with C/S was also previously shown by Garbev *et al.* [21] by XRD with synchrotron radiation. Black *et al.* [32] also showed an increase in structural ordering with C/S by X-ray photoelectron spectroscopy studies.

The change in basal spacing vs. C/S is plotted in Fig. 2. The actual C/S ratios of the samples were calculated as the average of several TEM-EDX point analyses and are published elsewhere [20]. The graph also shows data from a number of other studies, similar to that shown by Richardson [18], namely Matsuyama and Young [27], Grudemo [28], and Cong and Kirkpatrick [29]. It also includes the data for some of the C-(A)-S-H(I) structures of Richardson's recent model [18], which configures the middle trend line; the dimer, octamer, undecamer and infinite chain model structures are marked with crosses. The structures for the octamer and undecamer do not involve chains of 8 and 11 silicate tetrahedra, but rather interstratification of dimer and infinite-chain structures. As Richardson discussed, the difference in basal spacing from the samples that configure the data of the upper trend line and the lower trend lines comes from different water contents. Samples on the upper trend line have one water molecule more, per silicon atom, than samples on the lower trend line. Additionally, it is possible that a point that is close to the upper trend line also represents a mix of C-S-H and portlandite. The data points from the samples in this study fall mostly close to the upper trend line, suggesting a light degree of drying. The extent of drying for sample with C/S = 0.75 is higher than for the other samples, since the data point falls close to the intermediate trend line. The data point from the sample with bulk C/S=1.5 (marked with a white cross) is situated on the right side of the upper trend line. This agrees with the fact that other samples that showed presence of portlandite were also situated at the right side of the upper trend line. The data point of the sample with bulk C/S=1.33 is

also situated in the same area of the plot, despite the sample being portlandite free. However, this point is close to other data points from samples without portlandite that configure the upper trend line. It has to be noted that there may be uncertainties related to systematic and random errors in the C/S ratios and basal spacing of all the data in the graph, and this could explain why data from samples with portlandite and without it can be situated in a similar area of the plot.

### 3.2 Coupled TG/DSC/FTIR and *In situ* XRD

The TG mass loss data of as-prepared samples are shown in Fig. 3. The curves correspond to the typical dehydration of C-S-H in which the weight loss is maximal from room temperature to 200°C, and gradual for higher temperatures [9]. The samples exhibited total weight losses of 22-26%. The sample with bulk C/S of 1.5 also exhibited a weight loss step at  $\approx 400^\circ\text{C}$ , which corresponds to the dehydration of portlandite [26]. This step was not present for any other sample, which indicates that the samples were portlandite free up to bulk C/S=1.33, as was shown by XRD data in Fig. 1. Samples fabricated by Garbev *et al.* [9, 21, 32, 33] following a similar synthesis method were reported to be portlandite free up to bulk C/S=1.25. Differences in the drying method, or the use of ethanol, may have prevented the precipitation of portlandite in the sample with C/S=1.33. Portlandite probably precipitates while drying the sample when the solution is evaporating, increasing thus  $\text{Ca}^{2+}$  concentration. Rinsing the sample with ethanol removes most ions in solution, which could have prevented the formation of portlandite. Using high water to solid ratios in the order of 45-50 can also prevent the precipitation of portlandite and yield C-S-H with measured C/S ratios  $> 1.33$  [34-36].

The isoplots of XRD patterns in the range of the main C-S-H reflection (3.5 -2.6 Å) resulting from the in-situ XRD of the samples with bulk C/S=0.75, 1.0, 1.25 and 1.5 are

shown in Fig. 4 as a function of temperature. Samples with  $C/S=0.75$  and  $1.0$  showed a continuous transition with increasing temperature, with the main C-S-H reflection (regarded as 110), smoothly transitioning into reflection -2-22 of  $\beta$ -wollastonite (polytype 1A) at about  $800^\circ\text{C}$ . The decrease in intensity of the 110 reflection of the C-S-H with temperature was more pronounced for sample with  $C/S=1.0$  than  $0.75$ . This decrease was due to mainly two factors; increased thermal and structural disorder, and the collapse of the structure due to dehydration. Interestingly, the later prevailed. The collapse of the structure caused the main reflection to shift to lower interplanar distances ( $d$  in Fig. 4) leading to negative values in the linear coefficient of thermal expansion. In the case of  $C/S=0.75$  the resulting -2-22 reflection of wollastonite (1A) was the most prominent peak above  $800^\circ\text{C}$ , while sample with  $C/S=1.0$  also showed additional pronounced reflections ascribed to wollastonite. This was expected, due to the isochemical composition of C-S-H with  $C/S=1$  and wollastonite. The more rapid drop in intensity of the C-S-H 110 reflection observed for sample  $C/S = 1.0$  compared to  $C/S = 0.75$  suggests that the structure of C-S-H with lower  $C/S$  is more stable upon heating. This was further supported by the changes seen in the patterns from the sample with  $C/S=1.25$ . The XRD patterns for this sample showed a much quicker drop in intensity of the main C-S-H reflection with increasing temperature, such that between  $350^\circ\text{C}$  and  $800^\circ\text{C}$  there was almost no intensity observed in the range  $3.1\text{-}2.9 \text{ \AA}$ . These results indicate that long mean silicate chain lengths (MCL's) favor the stability of C-S-H. This supports the findings of others, who observed an increase in C-S-H stability with respect to calcium leaching in cement pastes containing 6% nanosilica [37] (hence C-S-H with long MCL and low  $C/S$ ). Above  $800^\circ\text{C}$ , in addition to the wollastonite reflections, reflections 611 and 031 of  $\alpha\text{-}C_2S$  (according to Mumme *et al.* [38]) were observed. The sample with  $C/S = 1.5$ , which contained an excess of portlandite,

revealed portlandite decomposition just above 400°C, manifested by the disappearance of the 100 and 101 reflections. Above 800°C a significant quantity of  $\alpha$ -L<sub>1</sub>C<sub>2</sub>S was detected, evidenced by its main reflections 611 and 031. In the transient zone between 600° and 800°C additional scattering was observed. Compared to the samples with lower C/S ratios, the formation of wollastonite occurred at significantly higher temperatures. A closer look at the XRD patterns obtained between 550 and 1050°C for sample with C/S = 1.5 is presented in Fig. 5. In the temperature range 650-800°C the additional scattering observed revealed reflections with low intensity, but which could be unambiguously assigned as -301, 002 and 121 of  $\beta$ -C<sub>2</sub>S. Reflection -301 was even still present at 850°C as a shoulder on the steadily growing 611 reflection of  $\alpha$ -L<sub>1</sub>C<sub>2</sub>S. The reflections of  $\alpha$ -L<sub>1</sub>C<sub>2</sub>S dominated the patterns obtained at temperatures higher than 800°C. Reflections due to rankinite, Ca<sub>3</sub>Si<sub>2</sub>O<sub>7</sub> or C<sub>3</sub>S<sub>2</sub>, (31-2 and 310) were transiently observed over the range 850 -1000°C, while formation of wollastonite was observed only above 900°C. Although not shown here, the progression of the basal reflection upon heating is similar to the 110 reflection. The basal spacing shifted to lower d values with increasing temperature. The reflection was visible up to 400°C for samples with low C/S and only visible up to approximately 200°C for C/S > 1. This can be explained by a rapid shrinkage of these later structures by the loss of water coordinating Ca<sup>2+</sup> in the interlayer.

The DSC data are shown in Fig. 6. These were dominated by the exothermal event corresponding to the transformation of C-S-H into  $\beta$ -wollastonite (800-900°C) and the endothermal transformation of  $\beta$ -wollastonite into  $\alpha$ -wollastonite (1220 -1280°C). It is obvious that there are not only differences in the position (in terms of onset temperature), but also in the shape of the DSC events. For example, the sample with C/S=0.75 showed a very high difference in the heat capacity before and after the

exothermal transformation ( $\Delta C_p$ ), which is mostly a reference for the equilibria of the ongoing reaction.  $\Delta C_p$  decreased with increasing C/S ratio approaching 0 (Fig. 7). This is possibly due to disequilibria caused by the presence of amorphous  $\text{SiO}_2$  for samples with  $C/S < 1$  accompanying the crystallization of  $\beta$ -wollastonite. When wollastonite ( $C/S = 1$ ) crystallizes by heating C-S-H with  $C/S < 1$ , there is an obvious excess of  $\text{SiO}_2$ . Amorphous  $\text{SiO}_2$  was detected in those cases as per XRD results reported by Garbev *et al.* [9]. With initial  $C/S > 1$ , there is an excess of CaO and  $\text{C}_2\text{S}$  was formed along with the crystallization of wollastonite, as shown earlier in the in-situ XRD patterns of samples with  $C/S=1.25$  and 1.5 (Fig. 4).

Table 1 displays the transformation temperatures vs. C/S for both the exothermal and endothermal events. The transformation of C-S-H into wollastonite occurred at higher temperature for higher C/S. This agrees with previously reported data on hydrothermally synthesized C-S-H by Mitsuda *et al.* [11] and Kalousek [10, 12], and with data by Garbev *et al.* [21] on mechanochemically synthesized C-S-H. Bornefeld [13] showed that the transformation temperature from C-S-H to  $\beta$ -wollastonite was an indication of the occupancy of the interlayer, since samples with  $C/S < 1$  and  $K/\text{Ca} = 0.25$ , with potassium most probably bonded in the interlayer, showed a similar transformation temperature than samples with  $C/S = 1.25$ .

A comparison of the transformation temperature data from this study with data from other authors is shown in Fig. 8. There was a fairly good agreement of all of the data for  $C/S > 0.7$ , including the data from the samples reported in this paper. For Mitsuda's samples, it is clear that the transformation temperature decreased up to  $C/S \approx 0.9$ , beyond which it started increasing with C/S ratio. This trend was not observed in any of the other samples. The disagreement of data from literature in the low C/S region may be due to differences in the samples, as for example different free silica content.

Garbev's samples were known to contain free silica at low C/S ratios [21] and their basal spacing may not have been as uniform as that in Mitsuda's samples, as these were hydrothermally synthesized.

Table 1. Temperature transformations for the exothermal event (C-S-H→ $\beta$ -wollastonite) and the endothermal event ( $\beta$ -wollastonite→ $\alpha$ -wollastonite) for C-S-H samples with bulk C/S indicated on the left column. The enthalpy of formation ( $\Delta H$ ) for CS, C<sub>2</sub>S and C<sub>3</sub>S<sub>2</sub> was calculated assuming the molar mass according to the composition of the C-S-H samples given in Table 4. Results noted with <sup>w</sup> relate to wet mass, i.e. including H<sub>2</sub>O; results marked with <sup>d</sup> relate to dry mass. The results were calculated as the mean and the standard deviation for the number of measurements indicated in column 7.

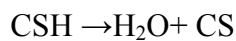
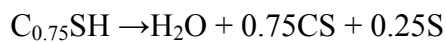
<b>Bulk C/S</b>	<b>T(°C)</b>	<b><math>\Delta H</math></b>	<b><math>\Delta H</math></b>	<b><math>\Delta H</math></b>	<b>T(°C)</b>	<b>No. of</b>
<b>M (g/mol) <sup>w(d)</sup></b>	<b>C-S-H→<math>\beta</math>- CS</b>	<b>CS (kJ/ mol)</b>	<b>C<sub>2</sub>S (kJ/ mol)</b>	<b>C<sub>3</sub>S<sub>2</sub> (kJ/ mol)</b>	<b><math>\beta</math>-CS→<math>\alpha</math>-CS</b>	<b>DSC  analyses</b>
<b>0.75</b>	820.4 ± 2.2	163 <sup>w</sup>			1280.6 ± 4.5	4
776.44 (587.77)		<b>123<sup>d</sup></b>				
<b>0.83</b>	827.3 ± 0.2	163 <sup>w</sup>			1277.5 ± 0.2	2
776.73 (570.27)		<b>120<sup>d</sup></b>				
<b>1</b>	833.5 ± 0.1	178 <sup>w</sup>			1247.8 ± 0.9	3
807.39 (584.55)		<b>129<sup>d</sup></b>				
<b>1.25</b>	877.5 ± 0.1	124 <sup>w</sup>	21 <sup>w</sup>		1239.8 ± 0.8	2
722.43 (547.39)		<b>94<sup>d</sup></b>	<b>16<sup>d</sup></b>			
<b>1.33</b>	896.1 ± 0.1	120 <sup>w</sup>	43 <sup>w</sup>		1234.9 ± 0.8	2
726.81 (556.01)		<b>92<sup>d</sup></b>	<b>34<sup>d</sup></b>			

<b>1.5</b>	$892.8 \pm 0.2$	$69^w$	$16^w$	$19^w$	$1228.4 \pm 1.5$	3
722.97 (561.17)		$53^d$	$12^d$	$15^d$		

The transformation temperature of  $\beta$ -wollastonite into  $\alpha$ -wollastonite (pseudowollastonite) increased with decreasing C/S, indicating that low C/S (excess of SiO<sub>2</sub>) stabilizes  $\beta$ -wollastonite while high C/S (excess of CaO) stabilizes  $\alpha$ -wollastonite. The reasons for this are not well known. It is possible that the silicate structure of the initial samples plays a role in determining this transformation temperature. The silicate structure of  $\beta$ -wollastonite is built by infinite chains while the silicate structure of  $\alpha$ -wollastonite comprises ternary [Si<sub>3</sub>O<sub>9</sub>] rings [39]. The silicate structure of the C-S-H samples with C/S > 1 is predominantly dimeric [20, 21, 32, 33], which go on to stabilize the ternary silicate rings of the  $\alpha$ -polymorph. Meanwhile, C-S-H samples with C/S < 1.25 consists of on average pentameric, or much longer silicate chains, up to  $\approx 20$  silicate tetrahedra [20, 21, 32, 33], and these samples stabilize the  $\beta$ -polymorph, which also comprises long silicate chains. It is plausible that there are small differences in the silicate structure of the  $\beta$ -polymorph that forms starting from low and high C/S ratio C-S-H, so that  $\beta$ -wollastonite is prone to transform to the  $\alpha$ -polymorph at different temperatures. This hypothesis would need further validation with a technique such as in-situ Raman spectroscopy, suitable to distinguish those minor structural differences in silicate anion structure. According to reported data, the temperature for this transformation increases with pressure [40, 41], and also depends on impurities. Rankin and Wright [42] investigated the ternary system CaO-Al<sub>2</sub>O<sub>3</sub>-SiO<sub>2</sub> and found that the transformation temperature from pure wollastonite to pseudowollastonite was 1200°C, while adding 10% of silica increased the transformation temperature by 10°C. Other mixtures of wollastonite, calcium silicates, calcium aluminate silicates and silica

decreased the transformation temperature. The progression of the transformation temperatures with C/S found in this work agrees with the results reported by Rankin and Wright. The greater the silica content, the higher the transformation temperature was, and the greater the CaO content, the lower the transformation temperature was. Therefore, the presence of other phases (SiO<sub>2</sub> or C<sub>2</sub>S) mixed with wollastonite, can also be responsible for the change in the transformation temperature from wollastonite to pseudowollastonite.

Table 1 gives an insight into not only the temperature dependence of the phase transformations observed, but also into the ΔH of the reactions involved. The values measured for all C-S-H phases with C/S <1 were very similar, which could be explained considering the equations:

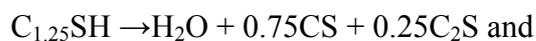


In fact, the only crystalline phase formed was wollastonite along with X-ray-amorphous SiO<sub>2</sub>. The lower Cp value for SiO<sub>2</sub> (quartz) at ~800°C (73.7 J/mol·K) compared to that of wollastonite (124.4 J/mol·K) is probably not relevant [43].

A comparison with the results from dehydration studies of the crystalline counterparts of C-S-H phases, 11Å tobermorite and xonotlite, performed by Shaw *et al.* [44] is of interest. 11Å tobermorite showed ΔH of 189 J/g or 138 kJ/mol at 857°C (main DSC peak). This result was obviously calculated considering a molar mass of 730.88g/mol; i.e. Ca<sub>5</sub>[Si<sub>6</sub>O<sub>17</sub>]·5H<sub>2</sub>O or wet mass. In order to compare with the result for C-S-H with C/S=0.83, the enthalpy of 189J/g was converted to that of the dry mass using the dry

mass of tobermorite (640.88 g/mol), and so obtaining a value of 121.1 kJ/mol. This is in good agreement with the value of 120 kJ/mol (Table 1). A comparison between the temperatures of wollastonite formation from C-S-H with C/S = 0.83 and tobermorite, shows the transition to be about 25°C higher for tobermorite, (Shaw *et al.* [44] gave only the temperature of the main peak and not of the onset). As Shaw *et al.* used a heating rate of 5°C/min, whilst the work in this paper used a heating rate of 10°C/min, this temperature difference should be even larger were the materials to be heated at the same heating rate. Therefore, the formation of wollastonite from C-S-H with C/S = 0.83 seems to be more favored than from its crystalline counterpart 11 Å tobermorite. Conversely, xonotlite showed a lower transformation temperature in the experiments from Shaw *et al.* [44] (815°C as peak center, onset well below 800°C) than C-S-H with C/S=1 (peak center at 835°C, onset at 833°C). In addition, the  $\Delta H$  of the transformation xonotlite  $\rightarrow$  wollastonite was lower (88J/g, 63kJ/mol for wet and 61.3kJ/mol for dry, respectively) than that for the C-S-H phase observed in this study (129 kJ/mol for dry).

Considering the C-S-H samples with C/S = 1.25 and 1.33, the reactions taking place upon heating could be represented as:



This is well reflected by the  $\Delta H$  values in Table 1. The sample with C/S = 1.5, which should behave as  $C_{1.5}SH \rightarrow H_2O + 0.5CS + 0.5C_2S$ , showed in turn partial formation of rankinite ( $Ca_3Si_2O_7$  or  $C_3S_2$ ) as an intermediate phase. Both  $C_2S$  (in its  $\beta$ - $C_2S$  and  $\alpha$ '- $C_2S$  forms) and rankinite, have higher  $C_p$  values than wollastonite in this temperature range (800-900°C) being around 184( $\pm$ 2) and 298( $\pm$ 2) J/mol·K, respectively [43]. An

interesting observation was that rankinite appeared to be an unstable phase upon dehydration of its isochemical counterpart  $C_{1.5}SH$ .

Another interesting point was the development of the FWHM (Full width at half maximum) of the exothermal event as a function of the C/S ratio (Fig. 9). The relatively broad effect shown by samples with C/S = 0.75 and 0.83 compared to 1.0 represents the different kinetics of wollastonite formation from C-S-H phases with different C/S ratios. For the latter sample, the conversion was rapid as the C/S ratio approached the ideal value of 1. For C/S > 1 an increase in the FWHM was observed indicating a slower rate of wollastonite formation. In addition, the formation took place at much higher temperatures as shown earlier.

The sample with C/S = 1.5 showed a lower FWHM than that with C/S = 1.33. This is in addition to the transition occurring at a lower temperature. A closer look at the DSC curves (Fig. 10) revealed a broad effect taking place at temperatures around 800°C, due to the formation of  $\alpha'_L-C_2S$  as shown by in-situ XRD (Fig. 4). The DSC curve for the sample with C/S= 1.5 showed an additional event at 850°C, due to rankinite formation [45], as confirmed by in-situ XRD (Fig. 5). Rankinite has a C/S of 1.5; thus, between C/S=1-1.5 there is increased competitive disequilibrium between the formation of  $C_2S$  and CS (wollastonite) [46]. Approaching C/S = 1.5, the composition allows the formation of rankinite, and a slightly accelerated formation of wollastonite took place again.

The traces for the H<sub>2</sub>O and CO<sub>2</sub> gases recorded by the coupled FTIR on the C-S-H samples are shown in Fig. 11, together with the simultaneously detected DSC and TG mass loss curves. From XRD (Fig. 1) the samples appeared not to be carbonated since there were no traces of calcite, aragonite nor vaterite in the XRD patterns. Similarly, TG

(Fig. 3) revealed no characteristic peaks resulting from the decomposition of vaterite or aragonite from 680°C to 780°, nor from the decomposition of calcite from 780 °C to 990°C (decomposition modes II and I according to Thiery *et al.* [47]). All the CO<sub>2</sub> that was released from the samples must have come from the decarbonation of small traces of amorphous carbonates. The CO<sub>2</sub> and H<sub>2</sub>O recorded for the first 2 minutes is an atmospheric residue due to the opening of the system to introduce the crucible. The water trace was very similar for all the samples, showing maximum release up to 200°C. The maximum release of H<sub>2</sub>O in this range shifted to higher temperatures with increasing C/S; an indication of more chemically bound water with increasing C/S. Only hard bound water remained in the structure after the samples were heated to 200 °C. A small release of water was also observed at the onset of the transformation to β-wollastonite for the samples with C/S=0.75 and 0.83. For the sample with bulk C/S = 1.5 there was also a release of water at ≈ 400°C; due to the dehydration of portlandite. The CO<sub>2</sub> traces showed similar shapes for the samples with C/S = 0.83, 1, 1.25, 1.33 with a broad event between 400°C and 600°C. Thiery *et al.* [47] associated a decomposition mode III to amorphous carbonates at temperatures between 550°C and 680 °C. Thus, the observed broad event was assigned to the decomposition of small traces of amorphous carbonates. The CO<sub>2</sub> traces also presented a sharp peak at the onset of the transformation to β-wollastonite; corresponding to the release of CO<sub>2</sub>. Two possibilities could account for this; the decomposition of nano-sized scawtite or spurrite that could have formed during heating of the samples, or the release of CO<sub>3</sub> groups that were trapped on surfaces of other phases. For the sample with bulk C/S of 0.75 there was also release of CO<sub>2</sub> between 300°C and 450°C. This temperature range is much lower to that of the decomposition mode III mentioned above, and therefore difficult to interpret. This release could be assigned to the decarbonation of amorphous

CaCO<sub>3</sub>(H<sub>2</sub>O). For the sample with bulk C/S = 1.5 the release of CO<sub>2</sub> at a temperature of ≈ 550°C could correspond to the decarbonation of cryptocrystalline (low crystalline) calcite that was possibly formed due to the carbonation of portlandite. The formation of other crystalline carbonates, such as aragonite and vaterite, could be excluded since they did not appear on the in-situ XRD isoplot below 550°C (not shown here), although amorphous traces of carbonates could have been present. The release of CO<sub>2</sub> before the transformation to β-wollastonite at ≈ 800°C can be associated with broad events found at the same temperatures in the DSC curves.

Table 2. Quantification of the release of CO<sub>2</sub> and H<sub>2</sub>O during thermal decomposition of C-S-H preparations: calculated as weight percentages from FTIR trace, the sum as total weight loss percentage from FTIR, total weight loss percentage from TG and calculated C/S from oxide mass balance as per TG results. The results were calculated as the mean and the standard deviation for the number of measurements indicated in column 6. C/S measured from TEM-EDX [20] is also added for comparison.

<b>Bulk C/S</b>	<b>CO<sub>2</sub> % content (FTIR)</b>	<b>H<sub>2</sub>O % content (FTIR)</b>	<b>Loss % (FTIR)</b>	<b>Loss % (TG)</b>	<b>No. of FTIR/TG curves</b>	<b>C/S (Mass balance)</b>	<b>Measured C/S (TEM)</b>	<b>No. of EDX points</b>
0.75	1.10 ± 0.11	23.20 ± 0.41	24.30 ± 0.44	24.19 ± 0.50	4	0.72	0.76 ± 0.02	20
0.83	1.18 ± 0.07	25.40 ± 0.08	26.58 ± 0.15	26.61 ± 0.16	2	0.80	0.79 ± 0.03	30
1.00	1.13 ± 0.04	26.47 ± 0.08	27.60 ± 0.05	27.56 ± 0.05	3	0.96	0.97 ± 0.05	25

1.25	0.68 ± 0.03	23.55 ±0.06	24.23 ± 0.03	24.22 ± 0.03	2	1.22	1.16 ± 0.06	21
1.33	1.11 ± 0.03	22.40 ± 0.36	23.50 ± 0.33	23.55 ± 0.30	2	1.29	1.24 ± 0.04	20
1.50	1.14 ± 0.03	21.25 ± 0.03	22.38 ± 0.06	22.46 ± 0.04	3	1.34	1.33 ± 0.07	30

The weight losses (as percentages) due to release of CO<sub>2</sub> and H<sub>2</sub>O were calculated by integrating the FTIR spectra and are shown in Table 2. The sum of evolved gases calculated from FTIR as total weight loss of the sample was compared with the loss calculated by TG (Table 2). The results from both techniques were very similar. This confirms the applicability of FTIR to analyze and quantify the gases based on a principal quantification method for coupled TG-FTIR-systems described by Merz *et al.* [23]. Coupled TG-FTIR proves to be an efficient tool evaluating the release of CO<sub>2</sub> and H<sub>2</sub>O from cementitious phases under thermal treatment. Thus, this technique could present an alternative to stand alone TG, adding information about the release kinetics and the chemical composition of the released gas mixture to the thermogravimetric data in a similar way to TG coupled with mass spectrometry. The actual C/S of the samples was calculated from oxide mass balance, taking into account the carbonates and portlandite content from TG (Table 2). All the calculated C/S ratios were very similar to the bulk compositions for the portlandite free samples (up to bulk C/S = 1.33). The actual C/S of C-S-H in the sample with bulk C/S = 1.5 is much lower than the bulk composition. This was due to the fact that some of the calcium added as a reactant was not incorporated into C-S-H, but rather precipitated as portlandite. The experimental C/S values from TEM-EDX [20] were similar to the ones obtained by mass balance,

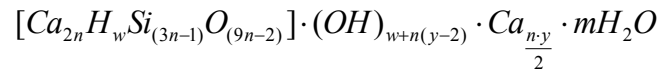
except for samples with bulk C/S = 0.75 and 1.25; however, given the error margin, they were considered to be in agreement.

### 3.3 Structural-chemical formulae for C-S-H(I)

Richardson and Groves' model was used to calculate the average composition of the samples. The model proposed a combination of T/J (tobermorite/jennite) or T/CH (tobermorite/calcium hydroxide) structural units. The formulations for the two viewpoints are described in refs.[15-17]. The applicability of the model to different systems is explained in detail in ref. [17]. A plot that is useful to assess whether the structures need Ca-OH bonds (jennite or calcium hydroxide units) is a representation of the C/S distribution vs. reciprocal MCL, together with the structural T and J units with maximum, intermediate and minimum degree of protonation ( $w/n = 2, 1, 0$ ;  $MCL = 3n - 1$ ;  $w =$  number of silanol groups) (See Fig.25 in ref. [17]). In this kind of plot, the tobermorite line with minimum degree of protonation ( $w/n = 0$ ) represents the maximum C/S ratios that the C-S-H structures can achieve without the presence of Ca-OH bonds, and hence without the need of jennite/calcium hydroxide. The C/S distribution from TEM-EDX of the studied samples was plotted vs. the reciprocal MCL (Fig. 12). The data were taken from ref. [20] and the mean value of the C/S was the one used to obtain the formulae (Table 2). This plot showed that the C-S-H samples could be entirely described by tobermorite units. This is in agreement with results by Raman spectroscopy studies of similar samples [33]. In addition to the lines that represent the T and J units with the different degrees of protonation, a dotted line representing the addition of one interlayer  $Ca^{2+}$  per vacant bridging tetrahedral site is also plotted. This line is a constraint that Richardson used to develop his model structures in the C-(A)-S-H(I) model. As can be seen in Fig. 12, the data from the samples fit very well with this

assumption. The C/S distributions cross the dotted line for all samples. In the case of low C/S even the mean C/S are very close to the dotted line.

The T/J viewpoint of Richardson and Groves' model was chosen because it is generally used when the samples can be expressed purely by tobermorite units, and these C-S-H samples were mostly portlandite free. The T/J formulation is:



The model parameters n and y can be calculated knowing the MCL (mean silicate chainlength) which is 3n-1, and the C/S. The amount of water (m) was calculated using the FTIR data for water loss in Table 2. For sample with C/S=1.5, the water content was not corrected for portlandite, since the water FTIR trace showed that the amount of water expelled from portlandite was minimal compared to that expelled from C-S-H. In the formula shown above, the Ca<sup>2+</sup> ions in the main brackets are part of the main layer while the Ca<sup>2+</sup> ions outside the brackets are a combination of interlayer charge balancing ions and others that are part of the main jennite-like structure (Si-O-Ca-OH). If no Ca-OH bonds are present in the structure; which was the situation for the samples studied here, these calcium ions are purely interlayer ones. The parameter w (number of silanol groups) depends on the value of y according to:

$$\begin{aligned} 0 \leq y \leq 2 &\rightarrow n(2-y) \leq w \leq 2n \\ 2 \leq y \leq 4 &\rightarrow 0 \leq w \leq 2n \\ 4 \leq y \leq 6 &\rightarrow 0 \leq w \leq n(6-y) \end{aligned}$$

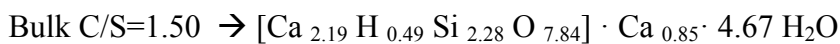
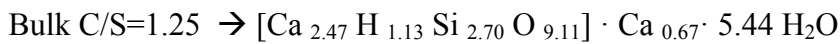
The calculated model parameters are shown in Table 3. The minimum degree of protonation ( $w/n_{\min}$ ) was chosen to calculate the structural-chemical formulae. It is a more suitable value than the maximum ( $w/n_{\max}$ ), according to the position of the mean

C/S data points with respect to the tobermorite trends in Fig. 12, since no CH or J units were needed.

Table 3. Calculated parameters of the T/J viewpoint of Richardson and Groves' model for the C-S-H samples. The amount of water  $m$  was calculated for the minimum degree of protonation.

<b>Bulk C/S</b>	<b>n</b>	<b>y</b>	<b>w<sub>min</sub></b>	<b>w/n<sub>min</sub></b>	<b>m(w<sub>min</sub>)</b>
0.75	7.36	0.36	12.07	1.64	32.51
0.83	3.83	0.31	6.46	1.69	18.75
1.00	2.20	0.98	2.23	1.02	12.50
1.25	1.23	1.08	1.13	0.92	5.44
1.33	1.17	1.34	0.78	0.66	5.15
1.50	1.09	1.55	0.49	0.45	4.67

The structural-chemical formulae of the mechanochemically synthesized C-S-H samples are:



The resulting structural chemical formulae comprised a tobermorite-like core (within brackets), with no extra Ca either in jennite or solid solution CH. Then all Ca outside the brackets was interlayer Ca. Samples with bulk C/S > 1 can be described by a combination of dimeric (T2) and pentameric (T5) tobermorite units. Samples with bulk C/S = 1 could be described by combinations of T5, T8 and T2 structural units. The sample with bulk C/S = 0.83 could be accounted for by a combination of T11 and the rest of the T units with shorter silicate chains, and the sample with bulk C/S = 0.75 could be described by a combination of T23 and the rest of the T units with shorter silicate chains.

According to these formulae the H<sub>2</sub>O:Si ratios of the samples are:

Bulk C/S=0.75 → H<sub>2</sub>O:Si = 1.83

Bulk C/S=0.83 → H<sub>2</sub>O:Si = 2.09

Bulk C/S=1.00 → H<sub>2</sub>O:Si = 2.43

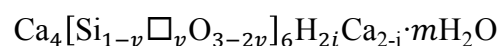
Bulk C/S=1.25 → H<sub>2</sub>O:Si = 2.22

Bulk C/S=1.33 → H<sub>2</sub>O:Si = 2.21

Bulk C/S=1.50 → H<sub>2</sub>O:Si = 2.15

These ratios correspond to a light degree of drying (See Fig 2. with the H<sub>2</sub>O:Si vs. C/S in [18]). They are in agreement with the conclusions drawn from Fig. 2 in which the basal spacing vs. C/S also suggested a light extent of drying.

The formulae can also be referred to 6 tetrahedral sites using the equivalent formulation of Richardson C-(A)-S-H(I) model for single-chain tobermorite or C-S-H(I):



Where  $v$  is the fraction of vacant tetrahedral sites and can be calculated knowing the MCL as:

$$v = \frac{1}{MCL + 1}$$

and  $i$  represents the extent to which the charge is balanced by protons or  $\text{Ca}^{2+}$  ions ( $i = 0, 1, 2$  for minimum, intermediate and maximum degree of protonation respectively)

and can be calculated knowing the C/S ratio and the fraction of vacant tetrahedral sites:

$$i = 6[1 - \left(\frac{C}{S}\right)(1 - v)]$$

The MCL and the C/S ratios were taken from [20] to calculate the model parameters.

The value of  $m$  was calculated taking into account the FTIR mass loss for water in

Table 2. The total water loss was considered, thus for sample with C/S = 1.5 no

correction for water content in portlandite was applied. The calculated values of the

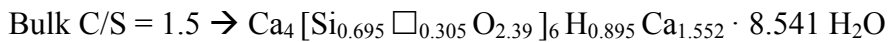
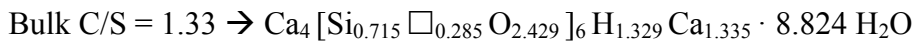
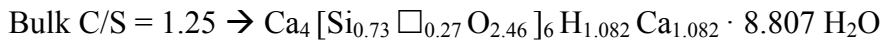
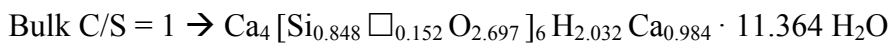
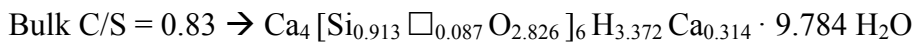
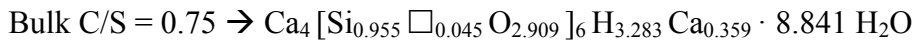
parameters  $v$ ,  $i$  and  $m$  are shown in Table 4, together with the number of interlayer  $\text{Ca}^{2+}$  ions per tetrahedral site.

Table 4. Calculated parameters of the C-(A)-S-H(I) formulation for the C-S-H preparations, together with the number of interlayer  $\text{Ca}^{2+}$  per tetrahedral site.

<b>Bulk C/S</b>	<b>v</b>	<b>i</b>	<b>m</b>	<b>Interlayer <math>\text{Ca}^{2+}</math> per tetrahedral site</b>
0.75	0.0453	1.641	8.841	0.060
0.83	0.087	1.686	9.784	0.052
1	0.152	1.016	11.364	0.164
1.25	0.270	0.918	8.807	0.180

1.33	0.285	0.665	8.824	0.223
1.5	0.305	0.448	8.541	0.259

The resulting structural-chemical formulae are as follows:



The formulae referred to 6 tetrahedral sites show that the interlayer  $\text{Ca}^{2+}$  per silicon tetrahedral site increased with C/S ratio. This can explain why samples with high MCL and low C/S are less prone to calcium leaching as found in [37], since the greater the amount of  $\text{Ca}^{2+}$  in the interlayer the more likely calcium leaching occurs. The higher occupancy of the interlayer with increasing C/S is also linked with the higher temperature needed for the transformation to wollastonite with increasing Ca content.

The MCL of the samples was plotted vs. C/S ratio in Fig. 13. The tobermorite trends for maximum, intermediate and minimum degree of protonation were also plotted (dashed lines). These lines can be expressed both in terms of the parameters of Richardson and Groves' and Richardson C-(A)-S-H(I) models and are equivalent to the lines that appear in Fig. 12. The left-hand dashed line represents the maximum degree of protonation ( $w/n = 2$  in Richardson and Groves';  $i=2$  in Richardson C-(A)-S-H(I) model):

$$\frac{C}{S} = \frac{\frac{2}{3}}{1 - v} = \frac{2n}{3n - 1}$$

The middle dashed line represents the intermediate degree of protonation ( $w/n = 1$ ;  $i=1$ ):

$$\frac{C}{S} = \frac{\frac{5}{6}}{1 - v} = \frac{\frac{5}{2}n}{3n - 1}$$

The right-hand dashed line represents the minimum degree of protonation or maximum C/S ratio ( $w/n = 0$ ;  $i = 0$ ):

$$\frac{C}{S} = \frac{1}{1 - v} = \frac{3n}{3n - 1}$$

The dotted line represents the case of the addition of one interlayer  $\text{Ca}^{2+}$  per vacant bridging tetrahedral site and is also equivalent to the dotted line in Fig. 12:

$$\frac{C}{S} = \frac{\frac{2}{3} + v}{1 - v} = \frac{2n + 1}{3n - 1}$$

Richardson found that most of the published data from C-S-H samples follow this expression and applied it as a constraint to develop the structures for his C-(A)-S-H(I) model [18]. Data from Haas [35], Cong and Kirkpatrick [29] and Chen [48] is also plotted for comparison. It is clear that the data from the samples described in this article is explained well in terms of the C-(A)-S-H(I) model, since they follow the dotted line, which thus provides a compelling alternative to the simple eye-guide that was used on a similar figure in a recent review article [49].

#### 4. Conclusions

The results presented in this paper show that the onset temperature for the transformation  $\text{C-S-H} \rightarrow \beta\text{-wollastonite}$  increased with C/S ratio. The transformation

from  $\beta$ -wollastonite to  $\alpha$ -wollastonite occurred at lower temperatures for samples with initial high C/S ratios. This implies an excess of CaO stabilized the  $\alpha$ -polymorph and the excess of  $\text{SiO}_2$  stabilized the  $\beta$ -polymorph. It is possible that the initial silicate structure of the samples plays a role in determining this transformation temperature, since the silicate structure of the  $\beta$ -polymorph is built by long silicate chains and it is stabilized by an excess of  $\text{SiO}_2$ , and hence C-S-H with long silicate chains, while the  $\alpha$ -polymorph has a silicate structure formed by rings of three silicate tetrahedra and it is stabilized by C-S-H samples with shorter chains (excess of CaO). Further research is needed to elucidate whether the silicate structure of the  $\beta$ -polymorph that forms upon heating C-S-H phases is different depending on the initial C/S ratios, causing the  $\alpha$ -polymorph to form at different temperatures. This hypothesis would need further verification with a technique such as in-situ Raman spectroscopy. Alternatively, the presence of  $\text{SiO}_2$  or  $\text{C}_2\text{S}$  could be the reason for this change in transformation temperature with C/S.

In-situ XRD patterns recorded while heating the C-S-H samples showed that samples with low C/S ratios were more stable upon heating. Samples with  $C/S < 1$  transformed into  $\beta$ -wollastonite and  $\text{SiO}_2$  upon heating, while samples with  $C/S > 1$  transformed into  $\beta$ -wollastonite and  $\alpha'_L\text{C}_2\text{S}$ . Additionally,  $\beta\text{-C}_2\text{S}$  and rankinite were also detected and decomposed before the appearance of  $\beta$ -wollastonite for sample with  $C/S = 1.5$ . The DSC curves of the heating process were dominated by the transformations  $\text{C-S-H} \rightarrow \beta$ -wollastonite and  $\beta$ -wollastonite  $\rightarrow \alpha$ -wollastonite, but also showed events for the appearance of  $\alpha'_L\text{C}_2\text{S}$  and rankinite. The difference in heat capacity before and after the transformation to  $\beta$ -wollastonite indicated there was more disequilibrium of the reaction for low C/S ratio. This disequilibrium was associated to the appearance of amorphous  $\text{SiO}_2$  for  $C/S < 1$ . The kinetics of this transformation were also studied comparing the

FWHM of the DSC event, and showed that the transformation accelerated up to  $C/S = 1$ ; composition at which the FWHM showed a minimum. This is due to the isochemical composition of wollastonite and C-S-H with  $C/S = 1$ . For higher  $C/S$  ratios, the transformation decelerated up to  $C/S = 1.25$ . Once the composition allowed the formation of rankinite, which has a  $C/S = 1.5$ , the transformation accelerated again.

It was shown that both Richardson and Groves' and Richardson C-(A)-S-H(I) models were suitable to describe the structure of the samples. Richardson and Grove's model yielded structural chemical formulae for the C-S-H samples that consisted of purely tobermorite units. In addition, FTIR was shown to be an alternative technique to TG, since its quantitative nature makes it possible to calculate the weight loss according to the acquired spectra for the evolved gases upon heating.

### **Acknowledgements**

Thanks are due to the European Commission for funding from the European Union Seventh Framework Programme (FP7 / 2007-2013) under *grant agreement 264448*.

### **References**

- [1] I.G. Richardson, G.W. Groves, Microstructure and microanalysis of hardened ordinary Portland-cement pastes, *Journal of Materials Science*, 28 (1993) 265-277.
- [2] I.G. Richardson, The nature of the hydration products in hardened cement pastes, *Cement & Concrete Composites*, 22 (2000) 97-113.
- [3] I.G. Richardson, The nature of C-S-H in hardened cements, *Cement and Concrete Research*, 29 (1999) 1131-1147.
- [4] E. Bonaccorsi, S. Merlino, A.R. Kampf, The crystal structure of tobermorite 14 Å (Plombierite), a C-S-H phase, *Journal of the American Ceramic Society*, 88 (2005) 505-512.
- [5] E. Bonaccorsi, S. Merlino, H.F.W. Taylor, The crystal structure of jennite,  $Ca_9Si_6O_{18}(OH)_6 \cdot 8H_2O$ , *Cement and Concrete Research*, 34 (2004) 1481-1488.
- [6] H.F.W. Taylor, Hydrated Calcium Silicates. Part I. Compound Formation at Ordinary Temperatures, *Journal of the Chemical Society*, (1950) 3682-3690.
- [7] J.A. Gard, H.F.W. Taylor, Calcium silicate hydrate II ("C-S-H (II)"), *Cement and Concrete Research*, 6 (1976) 667-677.

- [8] S. Lim, P. Mondal, Micro-and nano-scale characterization to study the thermal degradation of cement-based materials, *Materials Characterization*, 92 (2014) 15-25.
- [9] K. Garbev, M. Bornefeld, G. Beuchle, P. Stemmermann, Cell dimensions and composition of nanocrystalline calcium silicate hydrate solid solutions. Part 2: X-ray and thermogravimetry study, *Journal of the American Ceramic Society*, 91 (2008) 3015-3023.
- [10] G.L. Kalousek, Application of differential thermal analysis in a study of the system lime-silica-water, *Proceedings of the 3rd International Symposium on the Chemistry of Cement*, London 1954, (Cement and Concrete Association, London), (1954) 296-311.
- [11] T. Mitsuda, S. Kobayakawa, H. Toraya, Characterization of hydrothermally formed C-S-H, *Proc. Int. Symp. Chem. Cem.*, 8<sup>th</sup>, 3, 1986, pp. 173-178.
- [12] G.L. Kalousek, Tobermorite and related phases in the system CaO-SiO<sub>2</sub>-H<sub>2</sub>O, *J. Amer. Concr. Inst. (Proc.)*, 51 (1955) 989-1011.
- [13] M.J. Bornefeld, PhD Thesis, Ruprecht-Karls-University of Heidelberg, 2013.
- [14] H.F.W. Taylor, Proposed structure for calcium silicate hydrate gel, *Journal of the American Ceramic Society*, 69 (1986) 464-467.
- [15] I.G. Richardson, G.W. Groves, Models for the composition and structure of calcium silicate hydrate (C-S-H) gel in hardened tricalcium silicate pastes, *Cement and Concrete Research*, 22 (1992) 1001-1010.
- [16] I.G. Richardson, G.W. Groves, The incorporation of minor and trace-elements into calcium silicate hydrate (C-S-H) gel in hardened cement pastes, *Cement and Concrete Research*, 23 (1993) 131-138.
- [17] I.G. Richardson, Tobermorite/jennite- and tobermorite/calcium hydroxide-based models for the structure of C-S-H: applicability to hardened pastes of tricalcium silicate, beta-dicalcium silicate, Portland cement, and blends of Portland cement with blast-furnace slag, metakaolin, or silica fume, *Cement and Concrete Research*, 34 (2004) 1733-1777.
- [18] I.G. Richardson, Model Structures for C-(A)-S-H(I), *Acta Crystallographica Section B-Structural Science*, 70 (2014) 903-923.
- [19] P. Yu, R.J. Kirkpatrick, B. Poe, P.F. McMillan, X. Cong, Structure of calcium silicate hydrate (C-S-H): Near-, Mid-, and Far-infrared spectroscopy, *Journal of the American Ceramic Society*, 82 (1999) 742-748.
- [20] E. Tajuelo Rodriguez, I.G. Richardson, L. Black, E. Boehm-Courjault, A. Nonat, J. Skibsted, Composition, silicate anion structure and morphology of calcium silicate hydrates (CSH) synthesised by silica-lime reaction and by controlled hydration of tricalcium silicate (C3S), *Advances in Applied Ceramics*, 114 (2015) 362-371.
- [21] K. Garbev, G. Beuchle, M. Bornefeld, L. Black, P. Stemmermann, Cell dimensions and composition of nanocrystalline calcium silicate hydrate solid solutions. Part 1: Synchrotron-based x-ray diffraction, *Journal of the American Ceramic Society*, 91 (2008) 3005-3014.
- [22] F. Saito, G.M. Mi, M. Hanada, Mechanochemical synthesis of hydrated calcium silicates by room temperature grinding, *Solid State Ionics*, 101 (1997) 37-43.
- [23] D. Merz, H. Geisert, H. Seifert, J. Vehlow, Ammonia release in the thermal treatment of high-protein waste fractions, in: E. Kapsch (Ed.) *Hyphenated Techniques in Thermal Analysis : Proc. of the 3<sup>rd</sup> SKTBad Orb*, 2000, pp. 159-174.
- [24] R.S. Pease, An X-ray study of boron nitride, *Acta Crystallographica*, 5 (1952) 356-361.
- [25] H.E. Petch, Hydrogen positions in portlandite, Ca(OH)<sub>2</sub>, as indicated by electron distribution, *Acta Crystallographica*, 14 (1961) 950-957.
- [26] H.F.W. Taylor, *Cement chemistry*, 2<sup>nd</sup> ed., Thomas Telford, London, 1997.
- [27] H. Matsuyama, J.F. Young, Effects of pH on precipitation of quasi-crystalline calcium silicate hydrate in aqueous solution, *Advances in Cement Research*, 12 (2000) 29-33.
- [28] A. Grudemo, An electronographic study of the morphology and crystallization properties of calcium silicate hydrates, *Proc.– Swedish Cem. Conc. Res. Inst. Royal Inst. Technol., Stockholm*, (Handlinger–Svenska Forskningsinstitutet för Cement Och Betong vid Kungliga Tekniska Högskolan i Stockholm), 26 (1955) 1-103.

- [29] X. Cong, R.J. Kirkpatrick,  $^{29}\text{Si}$  NMR study of the structure of calcium silicate hydrate, *Advanced Cement Based Materials*, 3 (1996) 144-156.
- [30] G. Renaudin, J. Russias, F. Leroux, F. Frizon, C. Cau-dit-Coumes, Structural characterization of C-S-H and C-A-S-H samples-Part I: Long-range order investigated by Rietveld analyses, *Journal of Solid State Chemistry*, 182 (2009) 3312-3319.
- [31] S. Grangeon, F. Claret, C. Roosz, T. Sato, S. Gaboreau, Y. Linard, Structure of nanocrystalline calcium silicate hydrates: insights from X-ray diffraction, synchrotron X-ray absorption and nuclear magnetic resonance, *Journal of Applied Crystallography*, 49 (2016) 771-783.
- [32] L. Black, K. Garbev, G. Beuchle, P. Stemmermann, D. Schild, X-ray photoelectron spectroscopic investigation of nanocrystalline calcium silicate hydrates synthesised by reactive milling, *Cement and Concrete Research*, 36 (2006) 1023-1031.
- [33] K. Garbev, P. Stemmermann, L. Black, C. Breen, J. Yarwood, B. Gasharova, Structural features of C-S-H(I) and its carbonation in air - A Raman spectroscopic study. Part I: Fresh phases, *Journal of the American Ceramic Society*, 90 (2007) 900-907.
- [34] E. L'Hôpital, B. Lothenbach, D.A. Kulik, K. Scrivener, Influence of calcium to silica ratio on aluminium uptake in calcium silicate hydrate, *Cement and Concrete Research*, 85 (2016) 111-121.
- [35] J. Haas, A. Nonat, From C-S-H to C-A-S-H: Experimental study and thermodynamic modelling, *Cement and Concrete Research*, 68 (2015) 124-138.
- [36] C. Roosz, S. Gaboreau, S. Grangeon, D. Prêt, V. Montouillout, N. Maubec, S. Ory, P. Blanc, P. Vieillard, P. Henocq, Distribution of Water in Synthetic Calcium Silicate Hydrates, *Langmuir*, 32 (2016) 6794-6805.
- [37] J.J. Gaitero, W. Zhu, I. Campillo, Multi-scale study of calcium leaching in cement pastes with silica nanoparticles, *Nanotechnology in Construction* 3, Springer2009, pp. 193-198.
- [38] W. Mumme, L. Cranswick, B. Chakoumakos, Rietveld crystal structure refinements from high temperature neutron powder diffraction data for the polymorphs of dicalcium silicate, *Neues Jahrbuch fur Mineralogie Abhandlungen*, 170 (1996) 171-188.
- [39] Y.V. Seryotkin, E.V. Sokol, S.N. Kokh, Natural pseudowollastonite: Crystal structure, associated minerals, and geological context, *Lithos*, 134-135 (2012) 75-90.
- [40] I. Kushiro, Wollastonite-pseudowollastonite inversion, *Year Book - Carnegie Inst. Washington*, 63 (1964) 83-84.
- [41] W.L. Huang, P.J. Wyllie, Melting and Subsolidus Phase Relationships for  $\text{CaSiO}_3$  to 35 Kilobars Pressure, *American Mineralogist*, 60 (1975) 213-217.
- [42] G.A. Rankin, F.E. Wright, The ternary system  $\text{CaO-Al}_2\text{O}_3\text{-SiO}_2$ , *American Journal of Science*, (1915) 1-79.
- [43] C. Schmetterer, P.J. Masset, Heat Capacity of Compounds in the  $\text{CaO-SiO}_2$  System—A Review, *Journal of Phase Equilibria and Diffusion*, 33 (2012) 261-275.
- [44] S. Shaw, C.M.B. Henderson, B.U. Komarschek, Dehydration/recrystallization mechanisms, energetics, and kinetics of hydrated calcium silicate minerals: an in situ TGA/DSC and synchrotron radiation SAXS/WAXS study, *Chemical Geology*, 167 (2000) 141-159.
- [45] R. Della M., Studies in the System  $\text{CaO-Al}_2\text{O}_3\text{-SiO}_2\text{-H}_2\text{O}$ : III, New Data on the Polymorphism of  $\text{Ca}_2\text{SiO}_2$  and Its Stability in the System  $\text{CaO-SiO}_2\text{-H}_2\text{O}$ , *Journal of the American Ceramic Society*, 41 (1958) 293-299.
- [46] M. Dapiaggi, G. Artioli, C. Righi, R. Carli, High temperature reactions in mold flux slags: Kinetic versus composition control, *Journal of non-crystalline solids*, 353 (2007) 2852-2860.
- [47] M. Thiery, G. Villain, P. Dangla, G. Platret, Investigation of the carbonation front shape on cementitious materials: effects of the chemical kinetics, *Cement and Concrete Research*, 37 (2007) 1047-1058.
- [48] J.J. Chen, J.J. Thomas, H.F.W. Taylor, H.M. Jennings, Solubility and structure of calcium silicate hydrate, *Cement and Concrete Research*, 34 (2004) 1499-1519.

[49] B. Lothenbach, A. Nonat, Calcium silicate hydrates: Solid and liquid phase composition, Cement and Concrete Research, 78, Part A (2015) 57-70.

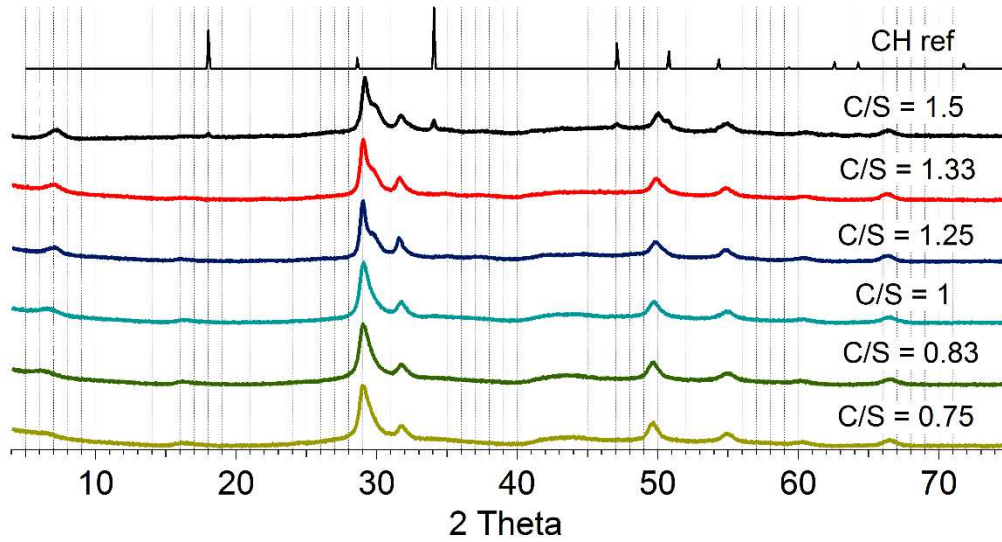


Fig. 1. XRD patterns of C-S-H samples synthesized via silica-lime reactions. The bulk C/S ratios of the samples are indicated over each pattern. A reference pattern from the Chemical Database service for portlandite is also shown.

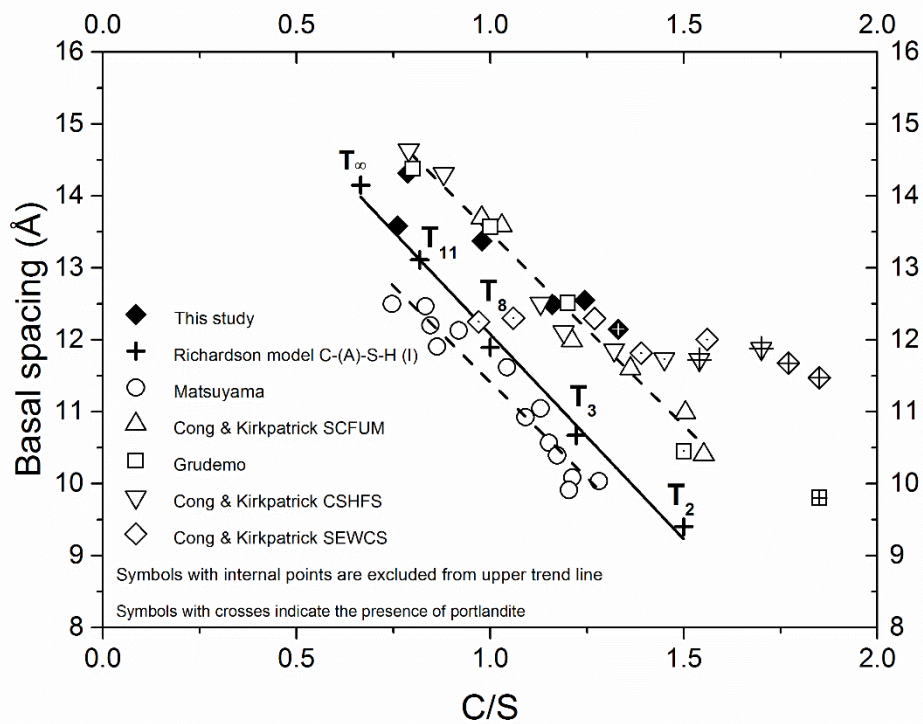


Fig. 2. Basal spacing vs. C/S ratio (TEM-EDX) [20] for the C-S-H samples. Data from other authors configure the trend lines. Symbols marked with points or crosses belong to the same data groups as the identical unfilled symbols and are not used to fit the trend lines. Crosses indicate presence of portlandite.

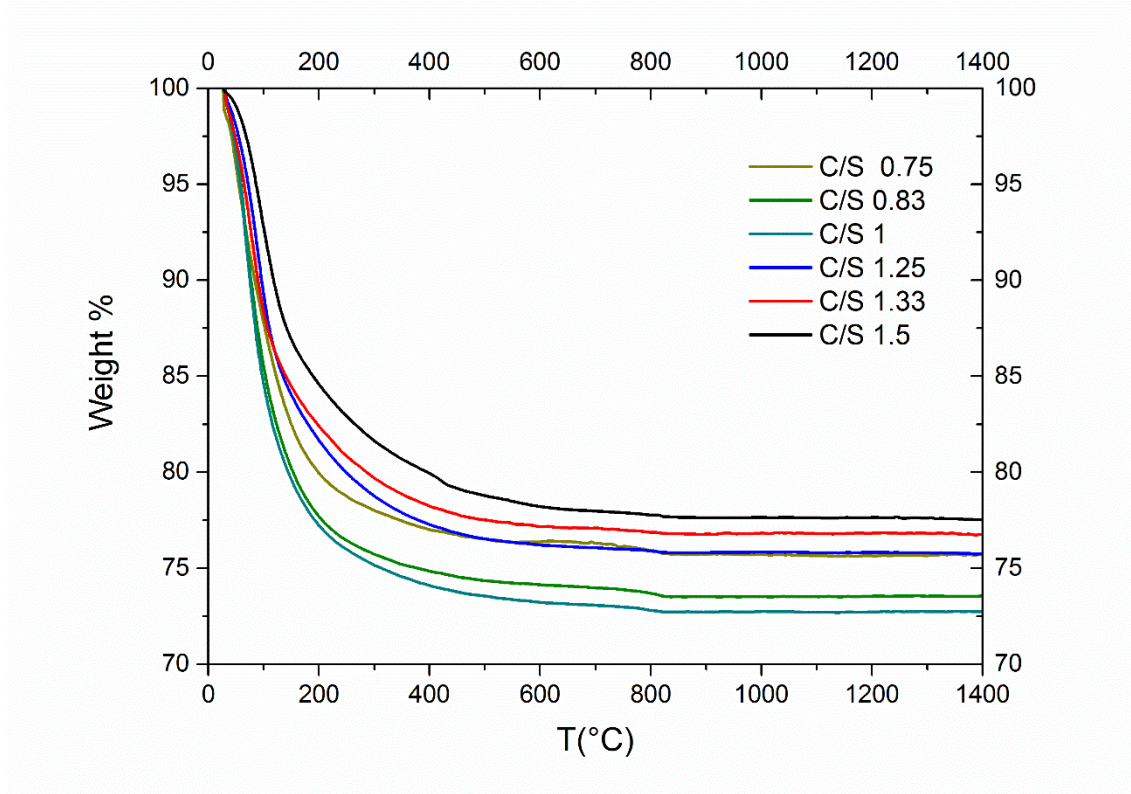


Fig. 3. TG traces from the C-S-H samples.

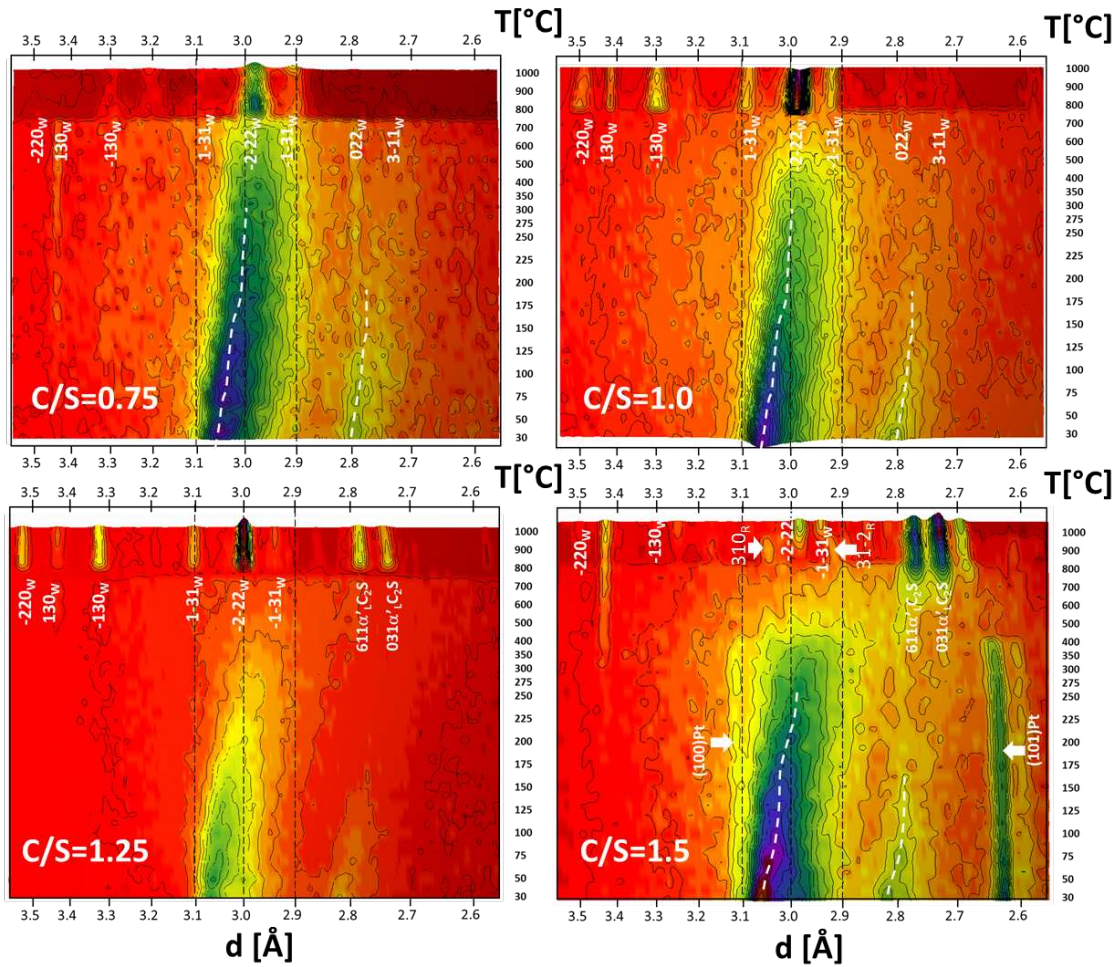


Fig. 4. In situ XRD patterns of C-S-H samples with bulk C/S = 0.75, 1, 1.25, 1.5 taken while heating from room temperature to 1000°C, showing the main C-S-H reflection 110 at  $\sim 3\text{\AA}$  transiting into the  $\beta$ -wollastonite reflection -2-22, the appearance of other  $\beta$ -wollastonite reflections (marked with W) and reflections from  $\alpha'$ - $\text{C}_2\text{S}$  for C/S > 1. Reflections from portlandite and rankinite that fade at high temperatures are also visible for C/S = 1.5 (marked as Pt and R respectively).

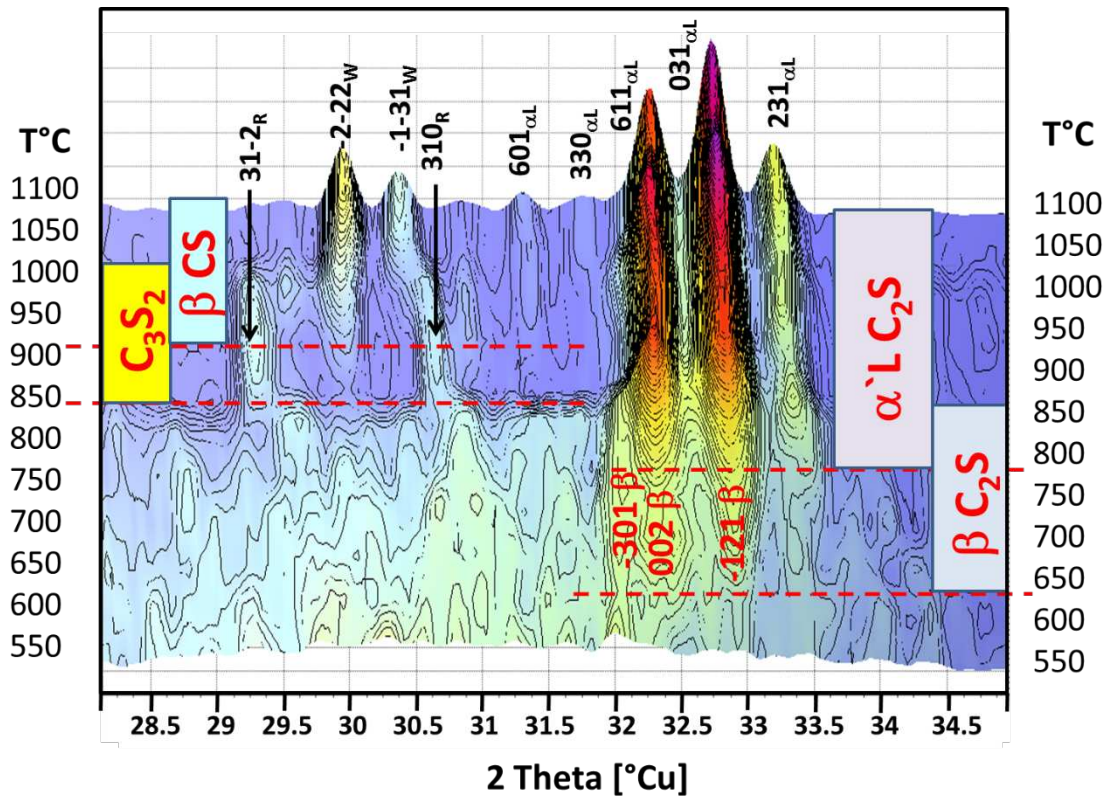


Fig. 5. Enlarged area of the in situ XRD patterns taken while heating C-S-H with bulk C/S = 1.5 in Fig.4, showing additional reflections from rankinite (C<sub>3</sub>S<sub>2</sub>) marked as R, and β-C<sub>2</sub>S, apart from the already identified reflections from β-wollastonite (β-CS) marked as W, and α'L C<sub>2</sub>S (marked as αL) in Fig. 4.

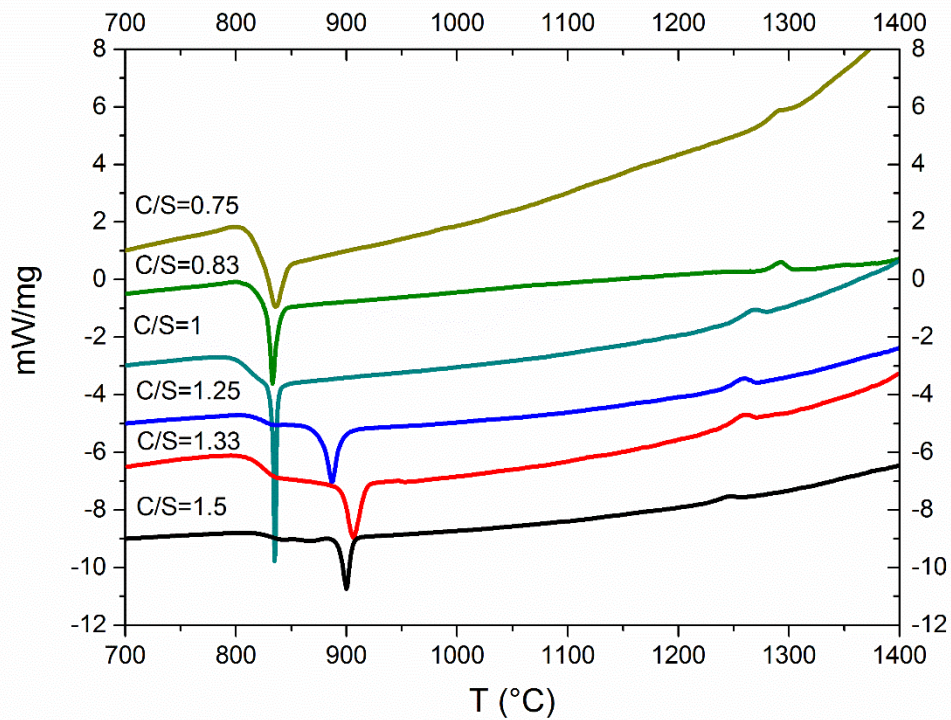


Fig. 6. DSC data of the C-S-H samples. The curves have been vertically shifted for clarity.

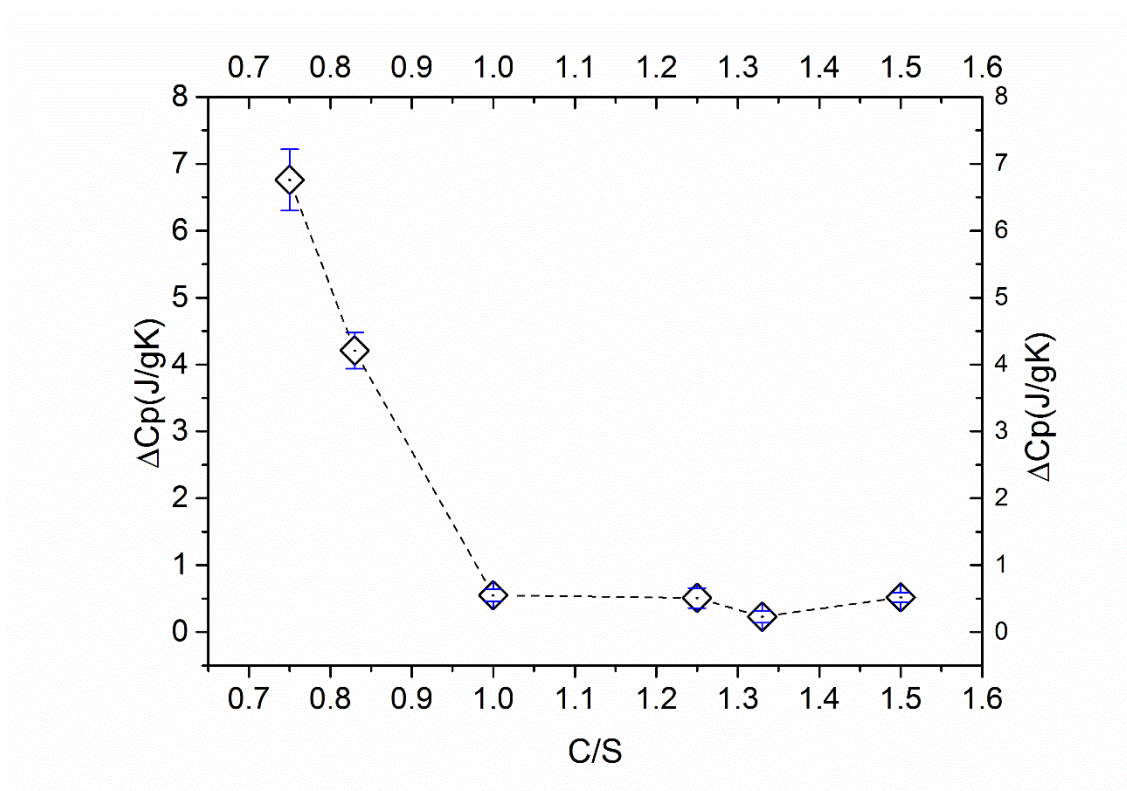


Fig. 7. Difference in heat capacity before and after the transformation of C-S-H into  $\beta$ -wollastonite vs. bulk C/S ratio. The units refer to grams of dried C-S-H.



Fig. 9. FWHM of the DSC event for the transformation C-S-H $\rightarrow$  $\beta$ -wollastonite vs. bulk C/S ratio of the C-S-H.

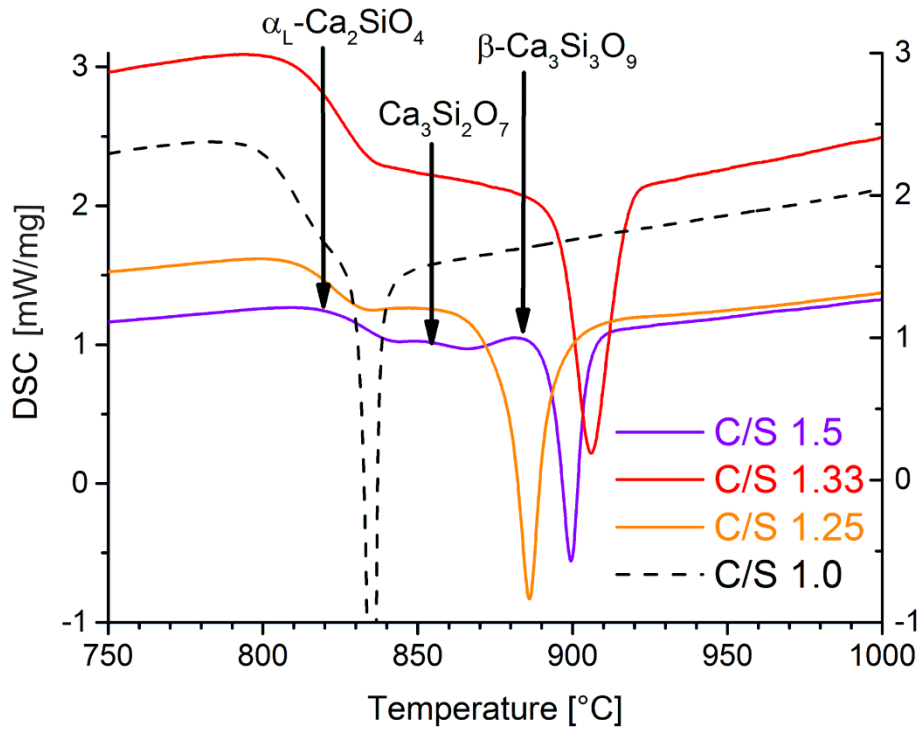


Fig. 10. DSC curves for the C-S-H samples with bulk  $C/S \geq 1$  in the region of the transformation C-S-H $\rightarrow$  $\beta$ -wollastonite. The formation of  $\alpha'_L\text{C}_2\text{S}$ , rankinite ( $\text{Ca}_3\text{Si}_2\text{O}_7$ ) and  $\beta$ -wollastonite are marked with arrows for sample with  $C/S = 1.5$ .

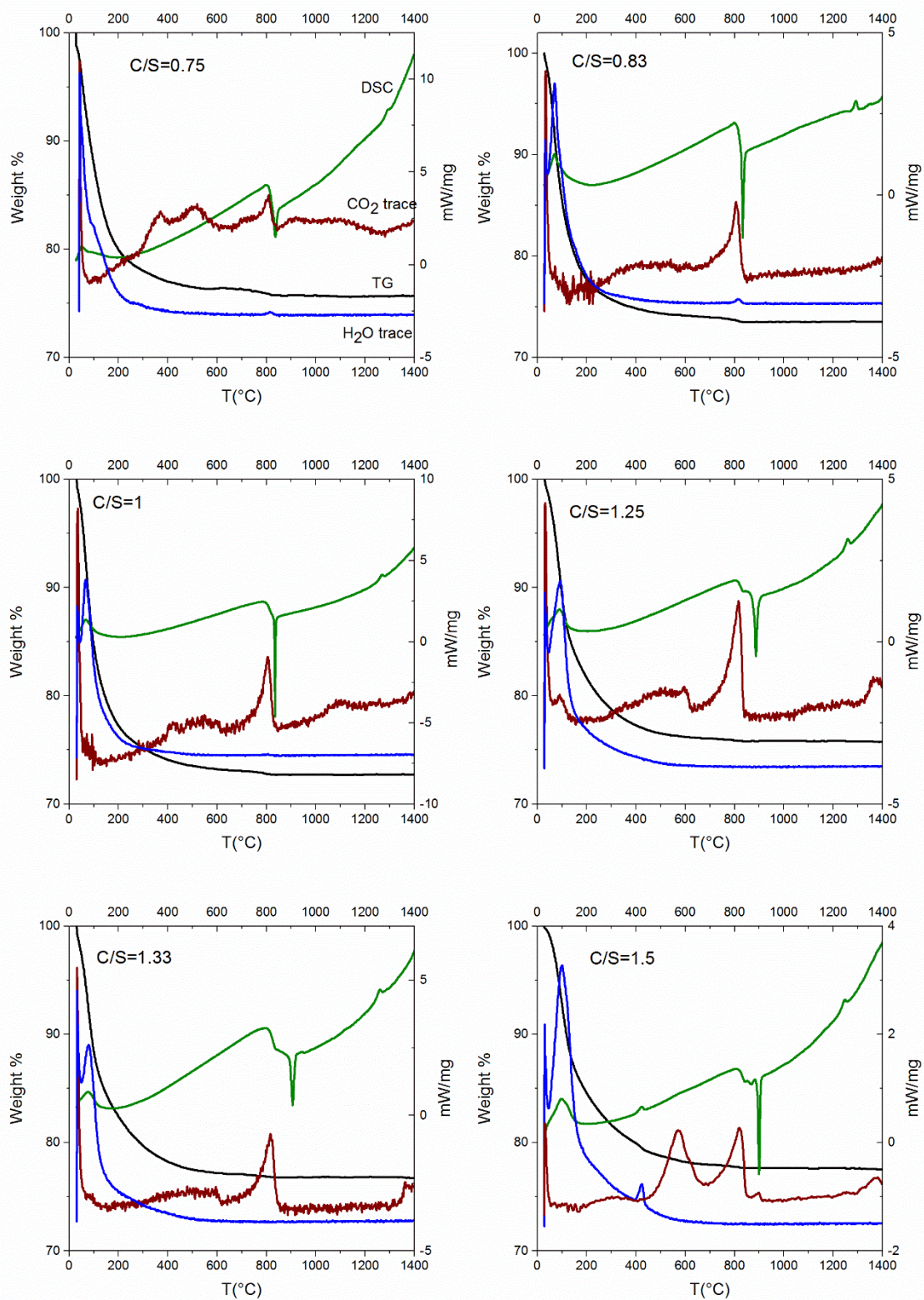


Fig. 11. Representation of the TG (black), DSC (green), and FTIR traces of H<sub>2</sub>O (blue) and CO<sub>2</sub> (red) of the C-S-H samples. The FTIR traces were normalized by sample weight. The scale of the y axis for the FTIR traces was chosen arbitrary for clarity and is not shown.

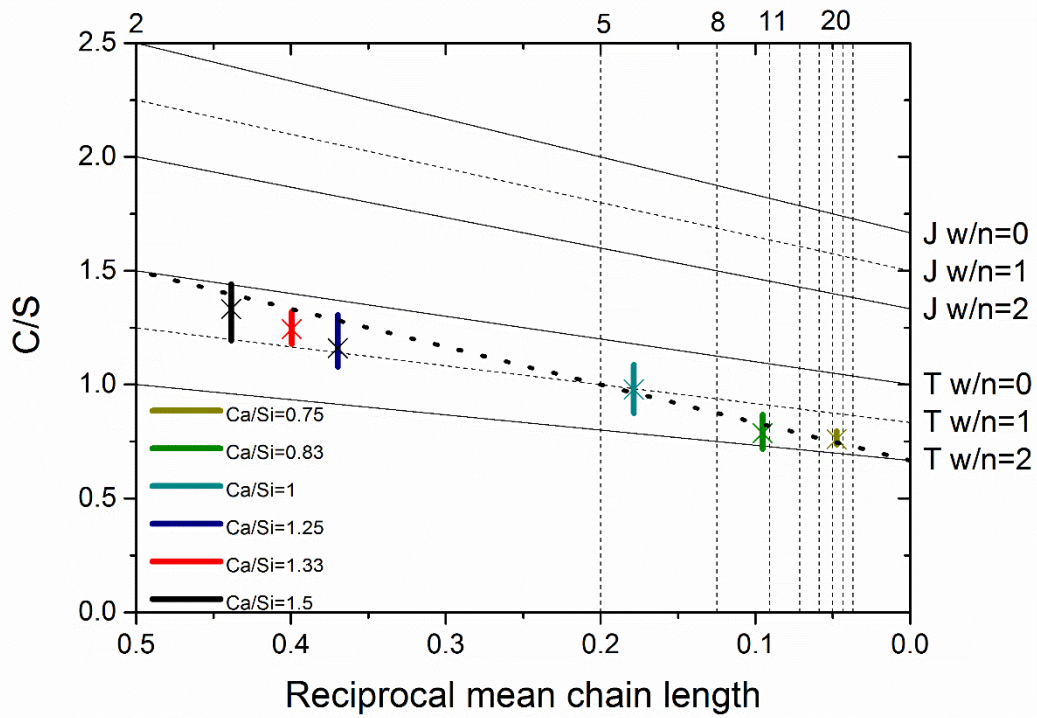


Fig. 12. C/S (TEM-EDX) [20] vs. reciprocal silicate mean chain length (Mean C/S marked with a cross over the C/S distribution represented by vertical bars) for the C-S-H samples. The structural units for tobermorite and jennite with minimum ( $w = 0$ ), intermediate ( $w = 1$ ) and maximum ( $w = 2$ ) degree of protonation are also marked. The vertical dashed lines represent the structural units: dimer (2), pentamer (5), octamer (8)...

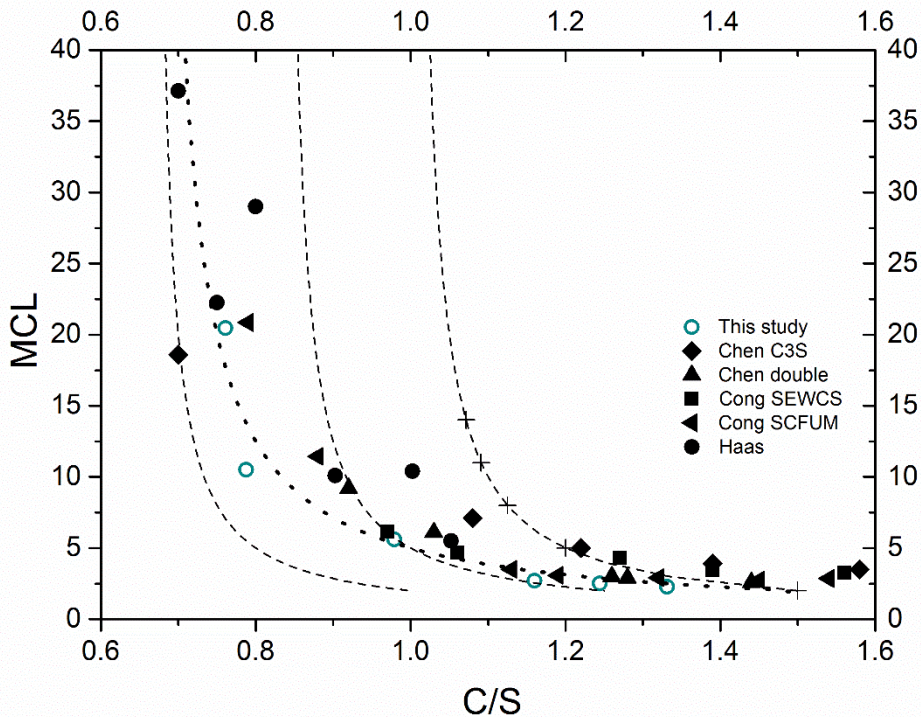


Fig. 13. Mean silicate chain length vs. C/S ratio (TEM-EDX) [20] of the C-S-H samples from this study and other authors. The dashed lines represent the tobermorite lines with maximum, medium and minimum degree of protonation (left to right) in Richardson and Groves' model. The crosses represent the T2, T5, T8, T11 and T14 structural units. The dotted line represents the constraint in terms of the fraction of vacant tetrahedral sites in Richardson C-(A)-S-H(I) model.